Simultaneous Spherical Crystallization and Co-Formulation of Drug(s) and Excipient from Microfluidic Double Emulsions

5 AUTHORS, INCLUDING:

Abu Zayed M Badruddoza
Massachusetts Institute of Technology

23 PUBLICATIONS **469** CITATIONS

Simultaneous Spherical Crystallization and Co-Formulation of Drug(s) and Excipient from Microfluidic Double Emulsions

Reno A. L. Leon,[†,⊥] Wai Yew Wan,[†,⊥] Abu Zayed M. Badruddoza,[†] T. A. Hatton,[‡,§] and Saif A. Khan*[,†,‡]

[†]Department of Chemical and Biomolecular Engineering, National University of Singapore, 4 Engineering Drive 4, Singapore 117576, Singapore

[‡]Chemical and Pharmaceutical Engineering Program, Singapore-MIT Alliance, National University of Singapore, 4 Engineering Drive 3, Singapore 117576, Singapore

[§]Department of Chemical Engineering, Massachusetts Institute of Technology, 77 Massachusetts Avenue, 66-309, Cambridge, Massachusetts 02139, United States

ⓢ *Supporting Information*
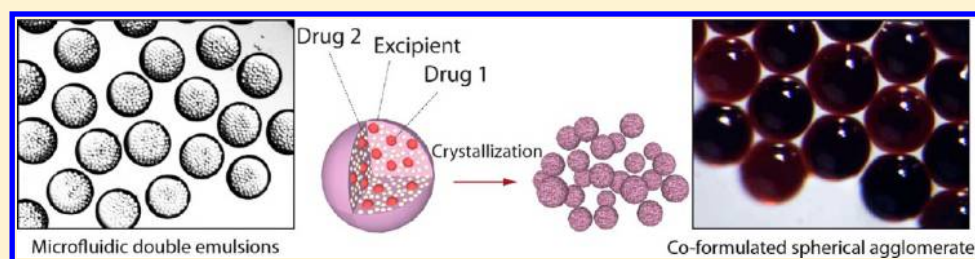
ABSTRACT: We demonstrate the fabrication of engineered pharmaceutical formulations of drug(s) and excipient as monodisperse spherical microparticles. Specifically, we fabricate monodisperse microparticles of ~200 μm size containing crystals of a hydrophobic model drug (ROY) embedded within a hydrophilic matrix (sucrose) (DE formulation), which in turn may also contain a hydrophilic model drug (glycine) (D^2E formulation). To do this, we dispense the components of the formulation into monodisperse oil-in-water-in-oil ($O_1/W/O_2$) double emulsions using capillary microfluidics, to subsequently enable simultaneous crystallization and co-formulation via solvent evaporation. We provide detailed morphological and polymorphic characterization of the particles obtained and highlight how (a) microfluidic methods enable formulations that are nearly impossible to achieve using conventional crystallization methods, and (b) these 'bottom-up' methods could potentially circumvent several energy intensive 'top-down' processes in traditional manufacturing, thereby offering the potential of continuous, sustainable pharmaceutical crystallization coupled with advanced formulations.

■ INTRODUCTION

Pharmaceutical formulation processes, in which active pharmaceutical ingredients (APIs) are blended with additives and excipients, are crucial downstream operations that not only dictate the final pharmacokinetic attributes of the product but also account for a significant fraction of the energy consumption in the entire manufacturing process. Most APIs are produced in crystalline form and undergo extremely energy intensive downstream operations such as comminution, milling, sieving, blending, and granulation, before tabletting into the final product. These steps are necessitated by poorly controlled primary crystallization processes that typically yield large crystals of irregular size and shape.

Comminution and high energy milling are energetically inefficient operations (process efficiencies are typically <5%) with associated drawbacks of contamination, amorphization, and polymorphic transformations.[1−3] After size reduction, API crystals are typically blended with suitable excipient(s) such as lubricants, fillers, binders, flavors, colors, and preservatives. Powder blending is stochastic in nature, and a unique set of process parameters must be determined for each set of

ingredients for optimal and uniform distributions; furthermore, separation and clustering of blended materials due to differences in size and density and interactions between API and excipients remain persistent challenges.[4−6] The penultimate step is granulation of blended ingredients to form agglomerates suitable for compaction. Dry granulation results in the formation of large amounts of dusts and also requires multistage compaction and sieving of its products,[7] thereby leading to increased process times and energy consumption, with an accompanying risk of dust explosions. Wet granulation, however, can only be performed on mixtures that are not moisture sensitive and may potentially cause polymorphic transformations of the API.[8]

To overcome some of these challenges, Kawashima and co-workers developed a technique to directly agglomerate crystalline material into spherical agglomerates (SAs) by the addition of a bridging liquid to a precrystallized broth.[9] These

agglomerates have improved micromeritic properties (such as powder packability and flowability), improved chemical stability and bioavailability, and can be directly compressed into tablets.[10,11] Such methods have also been used to accomplish formulations of API(s) and excipients.[12−14] Nevertheless, wide particle size distributions due to the inherently stochastic agglomeration phenomena and the requirement for compatible drugs and excipients (in terms of, for example, hydrophilicity) remain outstanding challenges in using such methods.

The central motivation of this work is therefore to demonstrate pharmaceutical formulation in bottom-up fashion, where crystallization and formulation occur in tandem, instead of via energy intensive top-down processes as described above (see Figure 1). We have recently demonstrated microfluidic
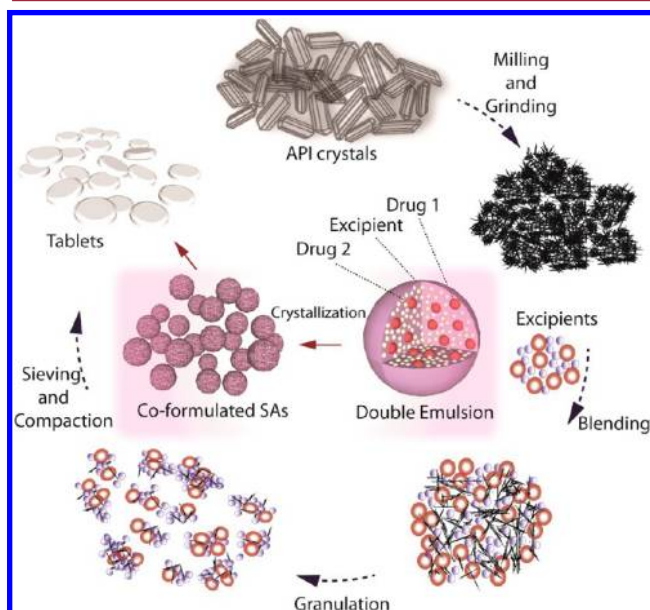

Figure 1. Schematic illustration of bottom-up approach (center) for co-formulation using double emulsions presented in comparison with contemporary pharmaceutical manufacturing steps (outer circle). Drug 1 (red) represents a hydrophobic API, while Drug 2 (yellow) represents a hydrophilic API, dispersed in a matrix comprising an excipient (pink).

emulsion-based spherical crystallization to fabricate monodisperse SAs of glycine.[15] In this article, we leverage another feature of microfluidic capillary-based emulsification, the ability to generate tightly controlled *multiple* emulsions,[16] to enable simultaneous crystallization and co-formulation of hydrophobic
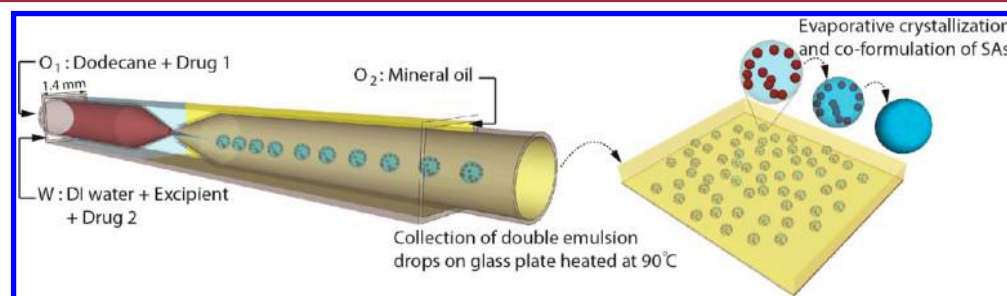
drug molecules within a hydrophilic matrix. Specifically, we use oil-in-water-in-oil ($O_1/W/O_2$) double emulsions to fabricate monodisperse microparticles of ∼200 μm size containing crystals of a hydrophobic model drug (ROY) embedded within a hydrophilic matrix (sucrose) (DE formulation), which in turn may also contain a hydrophilic model drug (glycine) (D^2E formulation), the first demonstration of its kind. We provide detailed morphological and polymorphic characterization of the particles obtained and highlight how (a) microfluidic methods enable formulations that are nearly impossible to achieve using conventional crystallization methods, and (b) these bottom-up methods could potentially circumvent several energy intensive top-down processes in traditional manufacturing, thereby enabling continuous, sustainable pharmaceutical crystallization coupled with advanced formulations.

■ EXPERIMENTAL SECTION

Materials. Glycine (>99%), dodecane (>99%), Span-80, trichloro-($1H,1H,2H,2H$-perfluorooctyl)-silane (97%), (3-aminopropyl)-triethoxysilane (97%), ammonium lauryl sulfate solution (ALS, 30% in water), n-hexane (HPLC grade, 95%), and mineral oil (light) were purchased from Sigma-Aldrich (Singapore) and used as received. Sodium dodecyl sulfate (SDS, 85%) was purchased from Merck (Germany). 5-Methyl-2-[(2-nitrophenyl)amino]-3-thiophenecarbonitrile (ROY) was purchased from Nanjing Chemlin Chemical Industry Co. Ltd., China. Ethyl acetate (99.9%) was purchased from Fischer scientific (Singapore). Ultrapure water (18.3 MΩ) obtained using a Millipore Milli-Q purification system was used to prepare aqueous glycine solutions. Harvard PHD 22/2000 series syringe pump was used for regulated flow at microliter scales. Square and cylindrical glass capillaries of ID 1 mm and 0.7 mm, respectively, were purchased from Arte glass associates Co., Ltd., Japan.

Methods. $O_1\backslash W\backslash O_2$ double emulsions were generated using a glass capillary microfluidic setup (see schematic in Figure 2). The axisymmetric coaxial glass capillary flow-focusing device was assembled using a square and two round capillaries. Round capillary 1 (C_1) (colored red in Figure 2) serves as the inlet for the inner fluid while round capillary 2 (C_2) (colored yellow in Figure 2) serves as the collection tube for the double emulsions. The square capillary was silanized with (3-aminopropyl)triethoxysilane (97%), and C_2 was silanized with trichloro-($1H,1H,2H,2H$-perfluorooctyl)-silane for hydrophilic and hydrophobic wetting properties, respectively, to aid in double emulsion generation. Ten microliters of either silane was used per glass capillary, and silanization was carried out for a minimum of 8 h in a vacuum chamber at a pressure of 0.08 MPa. The innermost oil phase (O_1) was prepared by mixing 1 parts ROY (30 mg/mL) in ethyl acetate solution with 5 parts dodecane containing 0.3% (w/w) surfactant, Span 80. Middle aqueous phase (W) was prepared by dissolving 1 g of sucrose, 100 mg of glycine, and 100 mg of surfactant (SDS) in 5 mL of ultra pure water for the D^2E formulation. Light mineral oil with 0.5% (w/w) of surfactant (Span 80) was used as the

Figure 2. Schematic of experimental setup depicting generation of $O_1/W/O_2$ (red/blue/yellow) double emulsion drops with multiple (n-in-1) inner O_1 droplets (red spheres) using capillary microfluidics, followed by evaporative crystallization of the formulated droplets on a heated glass plate to form SAs. Temporal progress of crystallization is represented as an increase in opacity of the W phase due to the presence of excipient.

continuous phase (O_2). O_2 and W phases were infused from the two ends of the square capillary through the outer coaxial region, while O_1 phase was infused through C_1 using syringe pumps (Harvard PHD 22/2000 series) at flow rates of 40, 7, and 1.8 μL/min, respectively. All the three fluids were hydrodynamically flow focused through the nozzle of C_2 resulting in the formation of the double emulsion drops. Approximately 1 mL of the double emulsion was collected on a glass slide spin coated with a thin layer of polydimethylsiloxane (PDMS) and subsequently heated at 90 °C on a hot plate (Thermo Scientific CIMAREC) for evaporative crystallization resulting in the formation of the formulated spherical agglomerates (SAs). High-speed real time imaging of the droplet breakup and stable emulsions collected on the glass slide was performed with high speed digital cameras (Basler pI640 or Miro Phantom EX2) mounted onto a stereomicroscope (Leica MZ16). A Leica CLS 150 XE light source was used.

Characterization. The size distribution, morphology, and polymorphism of the SAs obtained were characterized by using microscopic image analysis, field emission scanning electron microscopy (FE-SEM), powder X-ray diffraction (PXRD), and differential scanning calorimetry (DSC). For the size distribution studies we used an inverted microscope (Nikon Eclipse Ti) operated in bright field mode. The inbuilt software (NIS Elements 3.22.0) was used to measure the diameters of the agglomerates (circle by three-points method) and to estimate the average diameters and standard deviations based on measurements of at least 100 SAs. A field emission scanning electron microscope (JEOL JSM-6700F) at 5 kV accelerating voltage was used to acquire further structural information on the SAs. All samples were prepared on conventional SEM stubs with carbon tape and were coated with ~10 nm of platinum by sputter coating. An XRD diffractometer (LabX XRD-6000, Shimadzu) with characteristic Cu radiation was used for polymorphic characterization. The X-ray diffractometer was operated at 40 kV, 30 mA, and at a scanning rate of 2°/min over the range of $2\theta = 10-40°$, using the Cu radiation wavelength of 1.54 Å. The DSC thermograms were obtained using a Mettler Toledo DSC 882 apparatus. Around 10 mg of sample was crimped in a sealed aluminum pan and heated at 5 °C/min in the range of room temperature to 280 °C using an empty sealed pan as a reference. Dry nitrogen was used as purge gas and the N_2 flow rate was 50 mL/min. GC analysis was carried out on a Shimadzu GC 2010 Plus apparatus equipped with an auto injector (AOC-20i), flame-ionization detector and a separation column (30m, i.d. 0.25 mm). Around 10 mg of sample was crushed and added to 1 mL of hexane and loaded into the GC. The system was run for 8 min from 50 to 250 °C for a helium gas purge flow of 3 mL/min.

■ RESULTS AND DISCUSSION

We observed droplet generation in the microfluidic device using high speed imaging. A uniform stream of double emulsions with multiple inner droplets (*n*-in-1) (Figure 3a) is observed while operating in the jetting regime where droplet formation occurs downstream of the circular orifice of the collection tube. Jetting is a result of dominant viscous effects over inertial effects and interfacial forces; the viscosity of the outer O_2 phase is ~30 times that of the middle W phase.[16] The system operates at a low Reynolds number, as is characteristic of most microfluidic flow scenarios. The transition from the dripping to jetting regime is described by a Capillary number ($Ca = \mu V/\gamma) \approx 1$, where μ is the viscosity of the O_2 phase, V is a mean velocity of the inner W phase, and γ is the interfacial tension between the O_2 and W phases. The size of the middle and the inner phase droplets can be tuned by varying the flow rates of the respective fluids.[17] The volumetric flow rates of the O_2, W, and O_1 phases were set to 40, 7, and 1.8 μL/min, respectively. At these flow conditions, the frequency of droplet generation is 5 droplets per second (Figures 3b–e). The double emulsion drops (Figure 3f) have a mean diameter of 382 μm
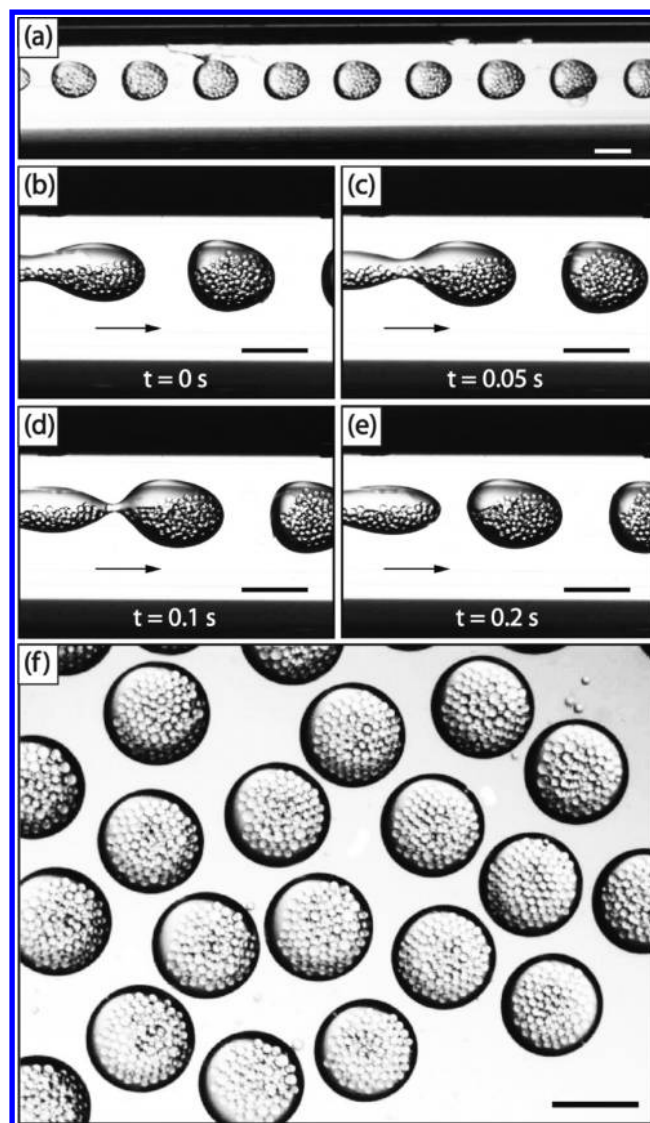

Figure 3. Stereomicroscopic images depicting (a) controlled generation of $O_1/W/O_2$ double emulsion drops, (b,c,d,e) time lapse images of double emulsion droplet break-up, and (f) collected double emulsions of the *n*-in-1 droplet morphology on a PDMS coated glass slide. All scale bars represent 300 μm.

with a standard deviation of 2%. A count of the number of inner O_1 droplets within these double emulsions gives $n = 85 \pm 8$ droplets. The diameter of the inner O_1 droplets is ~25 μm. By calculating the total volume of the O_1 droplets and the volume of the W phase, we estimate that ~45% of the droplet volume is occupied by the O_1 phase. A typical SA of the drug–drug–excipient (D^2E) formulation contains 1.3 μg of sucrose, 0.13 μg of glycine, and 0.03 μg of ROY, yielding a loading ratio of 40:4:1 (sucrose/glycine/ROY). Similarly, SAs of the drug–excipient (DE) formulation yield a loading ratio of 40:1 (Sucrose/ROY).

The presence of the O_1 and W phases allows for hydrophobic and hydrophilic APIs to be formulated as a single entity; a challenging task in contemporary pharmaceutical processing. The loading ratio of the APIs can also be monitored and controlled accurately. The concentration of the API in the O_1 or W phase can be regulated to increase or decrease the drug loading while the droplet morphology remains fixed. Alternatively, the loading can also be adjusted by altering the
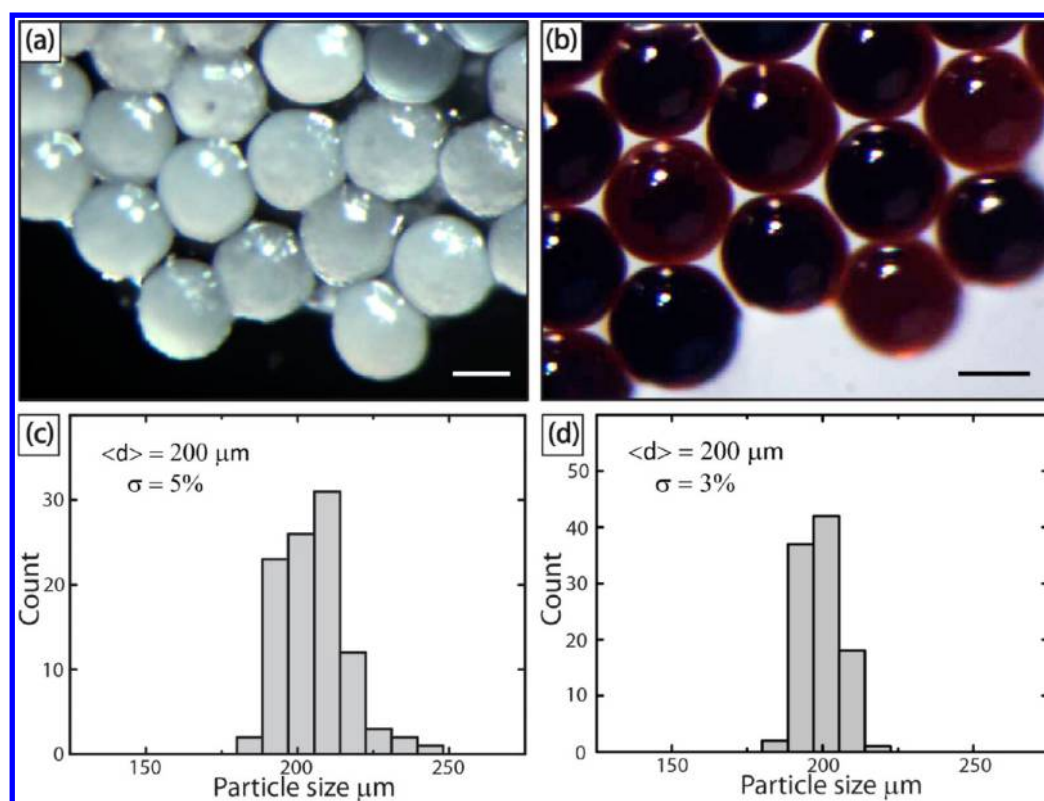
Figure 4. Stereomicroscopic images of DE (left column) and D^{2}E (right column) showing (a,b) monodisperse end products of crystallization (reflected light appears as white spots in both images) and (c,d) size distributions histograms of SAs. All scale bars represent 100 μm.

number of O$_1$ droplets or by varying the overall diameter of the double emulsion droplet. We were able to fabricate monodisperse SAs of both drug-excipient (DE) and drug–drug–excipient (D^{2}E) types with tunable particle sizes in the 100−300 μm range. Under the specific conditions noted in the experimental section, the mean particle sizes of the DE (Figure 4a) and D^{2}E (Figure 4b) SAs were ∼200 μm with a standard deviation of <5% (Figure 4c,d). This approach to monodisperse particulate formulations potentially circumvents several drawbacks in conventional processing, such as wide size distribution in batch crystallization, demixing in blending and challenges in the co-formulation of hydrophobic and hydrophilic APIs and excipients.[18−20] Finally, we note that the D^{2}E SAs appear brown on visual inspection (Figure 4b), possibly due to the Maillard reaction, which occurs when reducing sugars are formulated in the presence of amino compounds such as glycine.[21,22]

We observed several stages in the process of crystallization. First, the double emulsion droplets shrank to ∼60% of their original droplet diameter. Thereafter, a hard and brittle shell was observed to form at the W/O$_2$ interface, encapsulating the inner droplets (Figure 5a,b). Stereomicroscopic images obtained during the course of crystallization show the formation of a sucrose shell, while the O$_1$ droplets are still present (see Supporting Information, Section 1). Encapsulation is crucial in ensuring entrapment of the hydrophobic API in the event of coalescence of O$_1$ droplets with the O$_2$ phase. An increase in opacity of the encapsulated emulsions followed. The D^{2}E SAs appeared opaque due to the presence of glycine, while those of the DE SAs appeared translucent (Figure 5c,d).

Electron microscopy revealed that the surface of the DE SAs was smooth while that of the D^{2}E SAs was coarse (Figure 6a,b).
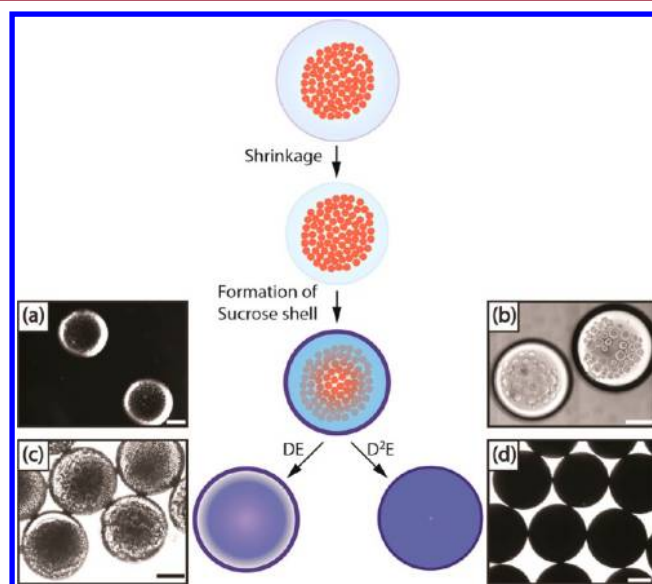

Figure 5. Schematic representation of the crystallization process and micrographs of DE (left column) and D^{2}E (right column) formulations showing initial shrinkage and generation of super-saturation prior to the formation of a sucrose shell at the onset of crystallization. Thereafter, either translucent SAs of the DE formulation or fully opaque SAs of the D^{2}E formulation are obtained. All scale bars represent 100 μm.

The smooth texture of the DE SAs is expected as it is typical of formulations containing sucrose.[23] However, on closer observation (Figure 6c), crystal facets of ∼2 μm were observed to populate the surface of the D^{2}E SAs; these facets can be attributed to the presence of glycine. Following the imaging of

D

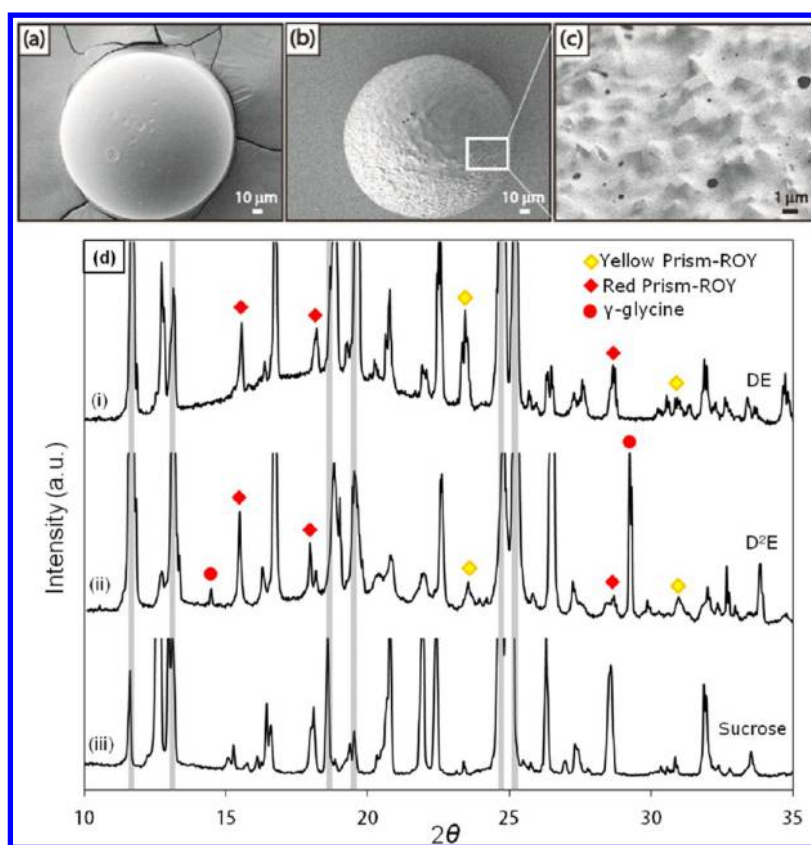dx.doi.org/10.1021/cg4012982 | *Cryst. Growth Des.* XXXX, XXX, XXX−XXX

Figure 6. Representative FESEM images and XRD characterization of spherical agglomerates from DE and D²E experiments: (a) SA of sucrose and ROY displaying a uniform and smooth surface; (b) SA of glycine, sucrose, and ROY exhibiting a rough surface with crystals packed together with sucrose, (c) close-up of faceted crystals located on the surface of the D²E SAs; (d) (i) XRD pattern of the DE SAs showing peaks corresponding to the yellow prism (Y) and red polymorph of ROY, (ii) XRD pattern of the D²E SAs showing peaks corresponding to the yellow prism (Y) and red polymorph of ROY and γ-glycine, and (iii) XRD pattern of crystalline sucrose. The regions where major peaks of crystalline sucrose reside are outlined with vertical gray lines.

the SAs of both experiments, we proceeded to corroborate the presence of glycine and ROY using XRD and DSC analysis. XRD reveals the presence of the yellow prism (Y) and red polymorphs of ROY and γ-glycine, respectively, as indicated in Figure 6d(i) and (ii); the observed characteristic peaks of ROY at 15.6°, 18.2°, and 23.8° provide strong validation for its presence within the SAs.[24,25] Other major peaks at 11.8°, 12.8°, 18.9°, 19.7°, 24.8°, and 25.2° may be attributed to the crystalline form of sucrose as shown in Figure 6d(iii).[26] Control experiments on ROY-containing *single* emulsion drops were performed to study and compare the polymorphic outcome. XRD characterization revealed that the yellow prism (Y) polymorph was the major component (see Supporting Information, Section 2), in agreement with previous studies that highlight the common occurrence of the yellow polymorph in a variety of crystallization conditions.[27,28] Interestingly, we obtained γ-glycine in our D²E formulations, as opposed to the more commonly obtained α-glycine in emulsion-based crystallization.[15] This can be attributed to the role of the sodium ions present in the surfactant used, sodium dodecyl sulfate (SDS). Sodium ions have been reported to inhibit the growth of metastable α-glycine via interaction with the carboxylate group of glycine zwitterions in solution, thus promoting the growth of γ-polymorph.[29] Control experiments using a different surfactant, ammonium lauryl sulfate (ALS), yielded α-glycine (refer Supporting Information, Section 2), thus confirming the role of SDS in the formation of γ-glycine

and thus demonstrating the possibility of polymorphic control using surfactants as additives.

DSC analysis further confirmed the presence of ROY. We identified 2 regions in the thermograms that corresponded to ROY and sucrose in both cases (Figure 7a,b). Among the observed peaks, an exotherm at 109 °C affirms the presence of yellow prism (Y) polymorph of ROY.[24] The next characteristic region of peaks is observed between 180 to 192 °C, which corresponds to the range that defines the decomposition temperature of sucrose. The exotherm observed at 160−170 °C for the D²E trials may be attributed to the decomposition temperature of glucose, a product of the hydrolysis of sucrose and precursor to the Maillard reaction. The peak position is characteristic of glucose decomposition for heating rates of 2−10 °C/min.[30] Lastly, the exotherm at 250 °C confirms the presence of glycine. The DSC results reinforce the XRD results, affirming successful co-formulation of the two drug models. In addition, we also studied the levels of residual solvent in the formulated SAs using GC analysis (refer Supporting Information, Section 3). Dodecane is the major component of the inner organic phase O₁, and its residual amount in the SAs was measured to be 7.5 μg/mg of SAs. This is well within the acceptable limits of residual solvents on typical paraffins under class 3 classification of residual solvents.[31]
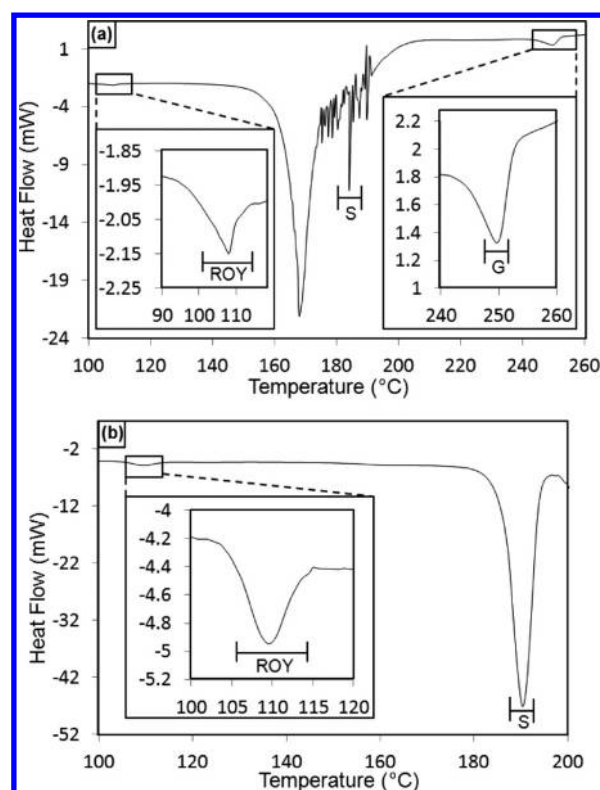
Figure 7. DSC profiles from (a) D²E and (b) DE cases: characteristic peaks are found in the vicinity of 109 °C (ROY), 180−192 °C (sucrose) and 250 °C (glycine), respectively. The exotherm between 160 and 170 °C for the D²E trials can be attributed to the decomposition temperature of glucose.[30]

CONCLUDING REMARKS

Our ongoing work beyond this initial proof-of-concept demonstration involves detailed studies of the dynamics of crystallization in this chemically complex emulsion system. The temporal stability of the inner O_1 phase and the influence of surfactants and excipient on the morphological and poly-morphic outcome are of particular interest. Furthermore, in such multicomponent systems, it is imperative to account for interactions between API(s) and excipient(s), such as the Maillard reaction mentioned above for the D²E particles and surface induced nucleation kinetics.[32] Finally, we note that the choice of the fluids used dictates the relative loading of APIs in the D²E system. This points to a potential limitation of our technique, in that the criteria for high loading of APIs (which depend on API solubility) and generation of robust, stable double emulsions (which depend on relative interfacial tensions) might not be met by the same set of fluids.

In summary, we have demonstrated a microfluidic method for co-formulation of hydrophobic and hydrophilic APIs in SAs with a narrow size distribution. This method, while still at the proof-of-concept stage, circumvents various energy-intensive processing steps of milling, blending, and granulation in traditional formulation routes. We envision that such methods, through further optimization, parameter space exploration, and especially through detailed engineering and feasibility studies of scale-up, can be made viable for the accelerated, energy- and cost-efficient production of designer pharmaceuticals that cannot be fabricated or formulated using traditional routes.

ASSOCIATED CONTENT

ⓢ Supporting Information

Additoinal experimental details. This material is available free of charge via the Internet at http://pubs.acs.org.

AUTHOR INFORMATION

Corresponding Author

*(S.A.K.) E-mail: saifkhan@nus.edu.sg.

Author Contributions

⊥These authors (R.A.L.L. and W.Y.W.) contributed equally to this work.

Notes

The authors declare no competing financial interest.

ACKNOWLEDGMENTS

REFERENCES

(1) Warman, M. Continuous Processing in Secondary Production. In *Chemical Engineering in the Pharmaceutical Industry*; John Wiley & Sons, Inc.: New York, 2010; pp 837−851.

(2) Bauer-Brandl, A. Polymorphic transitions of cimetidine during manufacture of solid dosage forms. *Int. J. Pharm.* **1996**, *140* (2), 195−206.

(3) Rhodes, M. Particle Size Reduction. In *Introduction to Particle Technology*; John Wiley & Sons, Ltd: New York, 2008; pp 311−335.

(4) Sindel, U.; Schweiger, A.; Zimmermann, I. Determination of the optimum mixing time for a mixture of lactose and colloidal silicon dioxide. *J. Pharm. Sci.* **1998**, *87* (4), 524−526.

(5) Ottino, J. M.; Khakhar, D. V. Mixing and segregation of granular materials. *Annu. Rev. Fluid Mech.* **2000**, *32*, 55−91.

(6) Chowhan, Z. T.; Chi, L. H. Drug-excipient interactions resulting from powder mixing III: Solid state properties and their effect on drug dissolution. *J. Pharm. Sci.* **1986**, *75* (6), 534−541.

(7) Tousey, M. D. The granulation process 101. *Pharm. Technol.* **2002**, 8−13.

(8) Wong, M. W. Y.; Mitchell, A. G. Physicochemical characterization of a phase change produced during the wet granulation of chlorpromazine hydrochloride and its effects on tableting. *Int. J. Pharm.* **1992**, *88* (1−3), 261−273.

(9) Kawashima, Y.; Okumura, M.; Takenaka, H. Spherical crystallization: Direct spherical agglomeration of salicylic acid crystals during crystallization. *Science* **1982**, *216* (4550), 1127−1128.

(10) Kawashima, Y.; Okumura, M.; Takenaka, H.; Kojima, A. Direct preparation of spherically agglomerated salicylic acid crystals during crystallization. *J. Pharm. Sci.* **1984**, *73* (11), 1535−1538.

(11) Bhadra, S.; Kumar, M.; Jain, S.; Agrawal, S.; Agrawal, G. P. Spherical crystallization of mefenamic acid. *Pharm. Technol.* **2004**, *28* (2), 66.

(12) Maghsoodi, M.; Taghizadeh, O.; Martin, G. P.; Nokhodchi, A. Particle design of naproxen-disintegrant agglomerates for direct compression by a crystallo-co-agglomeration technique. *Int. J. Pharm.* **2008**, *351* (1−2), 45−54.

(13) Pawar, A.; Paradkar, A.; Kadam, S.; Mahadik, K. Crystallo-co-agglomeration: A novel technique to obtain ibuprofen-paracetamol agglomerates. *AAPS PharmSciTech* **2004**, *5* (3), 57−64.

(14) Quon, J. L.; Chadwick, K.; Wood, G. P. F.; Sheu, I.; Brettmann, B. K.; Myerson, A. S.; Trout, B. L. Templated nucleation of acetaminophen on spherical excipient agglomerates. *Langmuir* **2013**, *29* (10), 3292−3300.

(15) Toldy, A. I.; Badruddoza, A. Z. M.; Zheng, L.; Hatton, T. A.; Gunawan, R.; Rajagopalan, R.; Khan, S. A. Spherical crystallization of

glycine from monodisperse microfluidic emulsions. *Cryst. Growth Des.* **2012**, *12* (8), 3977−3982.

(16) Utada, A. S.; Lorenceau, E.; Link, D. R.; Kaplan, P. D.; Stone, H. A.; Weitz, D. A. Monodisperse double emulsions generated from a microcapillary device. *Science* **2005**, *308* (5721), 537−541.

(17) Nisisako, T.; Okushima, S.; Torii, T. Controlled formulation of monodisperse double emulsions in a multiple-phase microfluidic system. *Soft Matter* **2005**, *1* (1), 23−27.

(18) Chadwick, K.; Davey, R. J.; Mughal, R.; Marziano, I. Crystallisation from water-in-oil emulsions as a route to spherical particulates: Glycine and the hydrochloride salts of glutamic acid and ephedrine. *Org. Process Res. Dev.* **2009**, *13* (6), 1284−1290.

(19) Hogg, R. Mixing and segregation in powders: evaluation, mechanisms and processes. *Kona* **2009**, *27*, 3−15.

(20) Hapgood, K. P.; Khanmohammadi, B. Granulation of hydrophobic powders. *Powder Technol.* **2009**, *189* (2), 253−262.

(21) Ellis, G. P. The maillard reaction. In *Advances in Carbohydrate Chemistry*; Melville, L. W., Ed.; Academic Press: New York, 1959; Vol. *14*, pp 63−134.

(22) Ferreira, V. F.; Nakamura, T.; Nakamura, M. K.; Ferreira, C. M. Sucrose hydrolysis without external acid catalyst. *An. Acad. Bras. Cienc.* **1990**, *62* (1), 13−15.

(23) Jovanović, N.; Bouchard, A.; Hofland, G.; Witkamp, G.-J.; Crommelin, D. A.; Jiskoot, W. Stabilization of proteins in dry powder formulations using supercritical fluid technology. *Pharm. Res.* **2004**, *21* (11), 1955−1969.

(24) Chen, S.; Guzei, I. A.; Yu, L. New polymorphs of ROY and new record for coexisting polymorphs of solved structures. *J. Am. Chem. Soc.* **2005**, *127* (27), 9881−9885.

(25) Li, H.; Stowell, J. G.; He, X.; Morris, K. R.; Byrn, S. R. Investigations on solid−solid phase transformation of 5-methyl-2-[(4-methyl-2-nitrophenyl)amino]-3-thiophenecarbonitrile. *J. Pharm. Sci.* **2007**, *96* (5), 1079−1089.

(26) Chinachoti, P.; Steinberg, M. P. Crystallinity of sucrose by X-ray diffraction as influenced by adsorption versus desorption, waxy maize starch content, and water activity. *J. Food Sci.* **1986**, *51* (2), 456−459.

(27) Chen, S.; Xi, H.; Yu, L. Cross-nucleation between ROY polymorphs. *J. Am. Chem. Soc.* **2005**, *127* (49), 17439−17444.

(28) Diao, Y.; Whaley, K. E.; Helgeson, M. E.; Woldeyes, M. A.; Doyle, P. S.; Myerson, A. S.; Hatton, T. A.; Trout, B. L. Gel-induced selective crystallization of polymorphs. *J. Am. Chem. Soc.* **2011**, *134* (1), 673−684.

(29) Towler, C. S.; Davey, R. J.; Lancaster, R. W.; Price, C. J. Impact of molecular speciation on crystal nucleation in polymorphic systems: The conundrum of γ glycine and molecular 'self poisoning'. *J. Am. Chem. Soc.* **2004**, *126* (41), 13347−13353.

(30) Hurtta, M.; Pitkänen, I.; Knuutinen, J. Melting behaviour of D-sucrose, D-glucose and D-fructose. *Carbohydr. Res.* **2004**, *339* (13), 2267−2273.

(31) Guideline for Residual Solvents Q3C(R5). In *International Conference on Harmonisation of Technical Requirements for Registration of Pharmaceuticals for Human Use*, 2011; pp 1−3.

(32) Diao, Y.; Myerson, A. S.; Hatton, T. A.; Trout, B. L. Surface design for controlled crystallization: The role of surface chemistry and nanoscale pores in heterogeneous nucleation. *Langmuir* **2011**, *27* (9), 5324−5334.